HHS Public Access

Author manuscript

Sci Signal. Author manuscript; available in PMC 2024 September 05.

Published in final edited form as:

Sci Signal. 2024 March 05; 17(826): eadd4671. doi:10.1126/scisignal.add4671.

Differential protein-protein interactions underlie signaling mediated by the TCR and a 4–1BB domain–containing CAR

Samuel A. Ritmeester-Loy[1], **Isabella H. Draper**[1], **Eric C. Bueter**[1], **Jonathan D Lautz**[1], **Yue Zhang-Wong**[2], **Joshua A. Gustafson**[2,3], **Ashley L. Wilson**[2,3], **Chenwei Lin**[4], **Philip R. Gafken**[4], **Michael C. Jensen**[2,3,5], **Rimas Orentas**[2,5], **Stephen E. P. Smith**[1,5,6,*]

[1]Center for Integrative Brain Research, Seattle Children's Research Institute, Seattle, WA 98101, USA.

[2]Ben Towne Center for Childhood Cancer Research, Seattle Children's Research Institute, Seattle, WA 98101, USA.

[3]Seattle Children's Therapeutics, Seattle Children's Research Institute, Seattle, WA 98101 USA.

[4]Proteomics and Metabolomics Facility, Fred Hutchinson Cancer Center, Seattle, WA 98101, USA.

[5]Department of Pediatrics, University of Washington, Seattle, WA 98101, USA.

[6]Graduate Program in Neuroscience, University of Washington, Seattle, WA 98101, USA.

Abstract

Cells rely on activity-dependent protein-protein interactions to convey biological signals. For chimeric antigen receptor (CAR) T cells containing a 4–1BB costimulatory domain, receptor engagement is thought to stimulate the formation of protein complexes similar to those stimulated by T cell receptor (TCR)–mediated signaling, but the number and type of protein interaction–mediating binding domains differ between CARs and TCRs. Here, we performed coimmunoprecipitation mass spectrometry analysis of a second-generation, CD19-directed 4–1BB:ζ CAR (referred to as bbζCAR) and identified 128 proteins that increased their co-association after target engagement. We compared activity-induced TCR and CAR signalosomes by quantitative multiplex coimmunoprecipitation and showed that bbζCAR engagement led to the activation of two modules of protein interactions, one similar to TCR signaling that was more weakly engaged by bbζCAR as compared to the TCR, and one composed of TRAF signaling complexes that was not engaged by the TCR. Batch-to-batch and inter-individual variations in production of the cytokine IL-2 correlated with differences in the magnitude of protein network activation. Future CAR T cell manufacturing protocols could measure, and eventually control, biological variation by monitoring these signalosome activation markers.

[*]Corresponding author. seps@uw.edu.

Author contributions: S.E.P.S. designed the study. S.R.-L., I.D., E.B., J.L., Y.Z.-W., J.G., and A.W. performed experiments. C.L., P.G., and S.E.P.S. performed and analyzed the MS experiments. M.J., R.O., and S.E.P.S obtained funding and designed the individual experiments. S.R.-L. and S.E.P.S. wrote the manuscript, and all authors read and approved the manuscript.

Competing interests: J.G. declares a consulting relationship with Tune Therapeutics. The other authors declare that they have no competing interests.

Introduction

Chimeric antigen receptors (CARs) use a single-chain variable antibody fragment (scFv) specific to tumor antigens to instruct T cell activation through an engineered construct containing CD3ζ and costimulatory domains(1, 2). Four CARs targeting CD19, using the costimulatory domains of either 4–1BB (tisagenlecleucel(3) and lisocabtagene maraleucel(4)) or CD28 (axicabtagene ciloleucel(5) and brexucabtagene autoleucel(6)) are FDA-approved for B cell lymphomas, and clinical trials have reported up to 94% remission rates after therapy(7). Despite these striking successes, many CAR design challenges remain. CARs are not very effective against solid tumors, which is likely due to the immunosuppressive tumor microenvironment, which prevents their more widespread use in oncology(8). The selection of appropriate tumor antigens is critical to prevent on-target, off-tumor side effects, and tumor heterogeneity or reduction in antigen abundance may lead to tumor escape and relapse. Even when a compatible tumor antigen is identified, as is the case with CD19 CARs, moderate-to-severe side effects, such as cytokine release syndrome or neurotoxicity, affect a substantial portion of patients, which prevents the use of CAR T cell therapy as a first-line treatment(9). Because the CAR is a synthetic receptor, it should be possible to bioengineer solutions to some of these issues. However, an engineering approach requires a solid understanding of the protein complexes that mediate downstream signal transduction and constitute the “programming language” of the cell(10).

The CAR is thought to instruct T cell activation by engaging protein-protein interactions similar to those engaged by the native T cell receptor (TCR)-CD3 complex in response to stimulation by peptide-bound major histocompatibility complex (pMHC)(1). In the TCR system, engagement of pMHC leads to the LCK- and FYN-dependent phosphorylation of CD3 immunoreceptor tyrosine-based activation motifs (ITAMs)—one each in CD3δ, CD3ε, and CD3γ, and three in CD3ζ—which recruit proteins containing Src homology 2 (SH2) and SH3 domains, such as the kinase ZAP70, in a phosphorylation-dependent manner(11). In addition, accessory binding sites on the TCR, such as the NCK-binding site in the proline rich region (PRR) of CD3ε(12), contribute additional complexity to the signalosome, rendering it sensitive to small changes in both pMHC binding kinetics and the costimulatory environment. The overall strength of signalosome activation appears to determine the cellular response(13). By contrast, the CAR contains only a single CD3ζ intracellular domain, which enables the CAR to bind to ZAP70 after scFv engagement, facilitating its phosphorylation and activation(14). However, mass spectrometry (MS) studies comparing the phosphoproteome after TCR vs. CAR stimulation found that key signaling adaptors downstream of ZAP70, including LAT and SLP-76, are phosphorylated to a much lower degree, or not at all, after CAR engagement as compared to after TCR engagement, suggesting less efficient signalosome formation(15, 16). In addition, the bbζCAR has a signaling motif that is not present in the TCR, which is derived from a TNF receptor family protein (TNFRSF9 or 4–1BB) that trimerizes in response to ligand binding to activate downstream extracellular signal-regulated kinase (ERK) and nuclear factor κB (NF-κB) signaling through a mechanism involving oligomerization of tumor necrosis factor (TNF) receptor–associated factors (TRAFs)(17). TRAFs are required for 4–1BB–mediated enhancement of bbζCAR function(18) through canonical or noncanonical nuclear factor

κB (NF-κB) pathways(19). However, the specific activity-dependent protein complexes recruited to the CAR after ligand binding, and their batch- and patient-specific variabilities, have not been thoroughly described.

We immunoprecipitated the bbζCAR from healthy donor–derived human CAR T cells and used MS to compare co-associated proteins before and after CAR stimulation. We identified 128 proteins that increased their co-association with the bbζCAR after stimulation by CD19, including ZAP-70 and a large TRAF signaling complex. We incorporated components of this bbζCAR signalosome into a quantitative multiplex co-immunoprecipitation (QMI) platform previously used to study dynamic protein-protein interactions downstream of TCR activation(13, 20) and compared signalosome formation after activation of the TCR vs. bbζCAR. We found a core network of interacting proteins that changed their pattern of co-association after CAR ligation, which varied in composition and intensity of activation between batches of CAR T cells produced from the same donor, CAR T cells using different scFv domains, and CAR T cells produced from different individuals. Our results support a model in which the bbζCAR recruits ZAP70, which stimulates the formation of a PI3K-LAT–SLP-76 signalosome that is quantitatively weaker than that induced by TCR stimulation, while simultaneously engaging TRAF-mediated complexes that include BIRC2/3 and TAK1. Batch- and patient-specific differences in the intensity of signalosome activation correlated with production of the cytokine interleukin-2 (IL-2), which suggests that variation in the expression or assembly of key signalosome components may contribute to variations in CAR performance.

Results

MS-based identification of signaling-induced protein complexes

To identify a bbζCAR-specific signalosome, we immunoprecipitated the protein complexes bound to the bbζCAR after ligand binding in primary human T cells and compared them to those immunoprecipitated in the basal (unstimulated) state. For maximal clinical relevance, we used CD4+ and CD8+ T cells from eight healthy donors lentivirally transduced in a GMP facility to express a clinical bbζCAR containing an anti-CD19 scFV, an IgG4 hinge, a CD28 transmembrane region, a 4–1BB costimulatory domain, the complete intracellular sequence of CD3ζ, and a T2A self-cleaving peptide that co-expresses a truncated EGFR marker and leaves a small “2A scar” on the C terminus of the mature CAR. In cells, this CAR forms a dimer through two cysteines in the IgG4 hinge domain and may additionally interact with itself or other proteins through the CD28 transmembrane domain(21) (Fig. 1, A and B). This CAR has undergone extensive clinical trials at our local institution (for example, NCT02028455)(7), and is identical to the FDA-approved lisocabtagene maraleucel(4) product.

To ensure robust detection of protein complexes and prevent occlusion of binding sites by the immunoprecipitating antibody, we performed two, independent MS experiments with two different immunoprecipitating antibodies, one against the C-terminal 2A scar (fig. S1A) and one against the N-terminal scFv domain (fig. S2A). Western blotting analysis demonstrated successful immunoprecipitation of the CAR, and co-immunoprecipitation of ZAP70 exclusively in the stimulated condition indicated successful detection of activity-

dependent protein complexes (figs. S1B and S2B). Furthermore, equal amounts of CAR were pulled down from the stimulated and unstimulated samples.

In the first experiment, one identical aliquot of CAR T cells mixed 1:1 with glutaraldehyde-fixed K562 cells stably expressing CD19 [which acted as antigen-presenting cells (APCs)] was incubated at 37°C for 5 min to induce signaling, and one identical aliquot was kept on ice (fig. S1A). Mock-transduced T cells were used as a negative control. This strategy ensured that the protein content of the CAR T cells and APCs were identical and enabled us to computationally subtract APC-derived proteins, such as CD19, which did not change in abundance with warming in fixed cells. To identify activity-dependent interactions, we compared proteins in the stimulated vs. unstimulated conditions for combined CD4+ and CD8+ T cells using a mixed linear model, and stringently removed “noise” proteins that appeared in >10% of human affinity purification experiments in the CRAPome database(22). Using cutoffs with a false discovery rate (FDR) < 0.1 and a $\log_2$ fold-change ($\log_2$FC) ≥ 1, we identified 67 proteins that were significantly increased in abundance after stimulation (Fig. 1C, fig. S1, and table S1). Note that ZAP70 was among the identified proteins ($\log_2$FC = 5.3, t = −2.77). The protein most significantly increased in abundance was BIRC3 ($\log_2$FC = 3.5, t = −3.58), an E3 ubiquitin ligase involved in TNF receptor family signaling. Ligand-induced trimerization of TNF-family receptors (such as 4–1BB) leads to the recruitment of BIRC3, and its homolog BIRC2, which ubiquitinate TRAF family proteins and recruit additional signaling molecules, including TAB1/2 and the kinase TAK1 (also known as MAP3K7), leading to the initiation of MAPK and NF-κB signaling(17). Six members of this signalosome were among our 67 identified ligand-dependent interactors: TRAF1 ($\log_2$FC = 4.4, t = −2.40), TRAF2 ($\log_2$FC = 7.4, t = −2.36), TRAFD1 ($\log_2$FC = 2.8, t = −2.01), BIRC2 ($\log_2$FC = 27.8, t = −2.52), BIRC3 ($\log_2$FC = 3.5, t = −3.58), and TAB2 ($\log_2$FC = 2.6, t = −2.01). Other notable proteins included PKCβ (KPCB, $\log_2$FC = 7.1, t = −3.19), a kinase that mediates the activation of NF-κB by phosphorylating CARD11/CARMA and forming a complex that includes TAK1(23); UBASH3A ($\log_2$FC = 5.9, t = −2.28), which regulates the ubiquitination and degradation of the TCR signalosome by inhibiting CBL-B(24); CD5 ($\log_2$FC = 2.1, t = −2.23), a negative regulator of TCR signaling that binds to CBL-B and UBASH3A, dampens NF-κB signaling, and promotes effector and memory cell phenotypes(25, 26); and CD44 ($\log_2$FC = 8.0, t = −2.92), a marker of memory/effector T cells that binds to LCK and may potentiate TCR responses by recruiting LCK to signaling sites(27).

It was somewhat surprising that we did not identify more TCR signalosome–associated proteins: LCK [$\log_2$FC = 2, t = −1.15; not significant (NS)], SLP-76 (not detected), LAT (not detected), GRAP2 ($\log_2$FC = 9.2, t = 1.19; NS), CD28 ($\log_2$FC = 1.03, t = −1.15; NS), and other major T cell signaling proteins did not reach statistical significance. We therefore performed a second experiment with two modifications to maximize our chances of identifying such interactions. First, we immunoprecipitated proteins with an anti-scFv antibody to ensure that signaling complexes were not occluding the 2A-binding site and preventing detection. Second, because cold treatment of T cells may cause TCR-like phosphorylation patterns that may mask CAR-induced signaling(28), we maintained all CAR T cells at 37°C and stimulated them with glutaraldehyde-fixed CD19-K562 cells or parental K562 cells as a stimulation control (fig. S2A). To differentiate proteins derived

from CAR T cells from those derived from APCs, we labeled the K562 cells with heavy isotope. We compared the stimulated vs. unstimulated conditions as described earlier, but used a 0.5 Log_2FC cut-off because of overall weaker induction of signaling complexes, and again removed noise proteins in the CRAPome database(22), as well as 33 proteins that were <75% heavy-labeled (derived from K562 cells). Note that CD19 was strongly enriched in the "stimulated" condition ($log_2FC = 5.05$, $t = -9.23$), but was 100% heavy-labeled (fig. S2, C and D). We identified 74 T cell–derived proteins that were significantly increased in abundance after stimulation (Fig. 1D, fig. S2, and table S1), including eleven proteins that were identified in both experiments: two that were previously linked to TCR signaling (ZAP70 and UBASH3A), two were linked to TNF receptor superfamily signaling (TRAF1 and TRAF2), and six that were linked to vesicle trafficking (AP2M1, FLOT1, and FLOT2) and the actin cytoskeleton (SMTN, GSN, and PPP1R18). Other notable proteins identified in this second experiment included TAB1 ($log_2FC = 1.78$, $t = -2.34$), a regulatory subunit of the kinase TAK1(29); TRADD ($log_2FC = 0.61$, $t = -2.14$), a negative regulator of TRAF signaling(30); and PKCθ ($log_2FC = 0.83$, $t = -2.27$), a kinase that mediates a prosurvival signal in T cells(31) and modulates the strength of TCR activation through the degradation of CBL-B(32). However, many classical TCR signalosome–associated proteins, including SLP-76, LCK, LAT, and GRAP2, were not detected.

We combined both datasets and used Gene Ontology (GO) and KEGG analysis to identify key cellular processes engaged by the CAR (table S2). Enriched GO terms included Actin Cytoskeletal organization ($P = 1.38 \times 10^{-12}$), actin-based filament transport ($P = 1.25 \times 10^{-5}$), positive regulation of NF-κB activity ($P = 1.49 \times 10^{-6}$), and early endosomal recycling and transport ($P = 0.0214$), whereas the KEGG pathways included NF-κB signaling ($P = 7.34 \times 10^{-08}$), TNF signaling ($P = 0.00016$), MAPK signaling ($P = 0.0071$), and TCR signaling processes ($P = 0.02$). We next used the PICKLE database(33) to visualize previously reported protein-protein interactions among all 128 of the proteins identified in both experiments (Fig 1E) and included known TNFRSF9 and CD3ζ interactions to represent the bbζCAR. Clusters of highly interconnected proteins included those involved in TRAF signaling, Ras/Rac/CDC42 signaling and actin mobilization, and clathrin-mediated endocytosis, as well as several kinases and nuclear-associated proteins. Overall, the interactors identified highlight extensive cytoskeletal rearrangements, the activation of TRAF-mediated signaling complexes, and ZAP70-mediated interactions not traditionally associated with TCR signaling.

Development of a quantitative multiplex coimmunoprecipitation (QMI) assay targeting bbζCAR signaling

Quantitative multiplex coimmunoprecipitation (QMI) is an emerging proteomic method that uses multiple color-classes of antibody-coupled flow cytometry beads to immunoprecipitate protein complexes, as well as fluorophore-coupled probe antibodies to monitor acute changes in 400+ binary protein-protein interactions during signaling events (Fig. 2A) (20, 34). To maximize protein complex detection in the CAR signalosome, we added several of the most connected nodes (Fig. 1E) to our previously described TCR signalosome panel(13, 20): CAR (anti-2A scar), TRAF1, TRAF2, and BIRC3. We also included three proteins that did not reach statistical significance in the MS experiments but are important to the

TRAF and NF-κB signalosomes in lymphocytes: TAK1 (MAP3K7, FC = 597, t = −1.09; NS), which is recruited by TAB1/2, signals to IKKβ(17), and is critical to interferon-γ (IFN-γ) production by CD8+ T cells(35); TNIK (found in only one co-IP experiment) which binds to TRAFs, may recruit NCK to link TRAFs with TCR signaling mechanisms(12), and is critical for the generation of CD8+ memory T cells(36); and SHARPIN (FC = 13.6, T = −1.21), a component of the linear ubiquitination complex (LUBAC) that promotes activation of the IKK complex downstream of TNF family receptors(37, 38), ubiquitinates the CARMA-BCL10-MALT complex(39), and may bind directly to TRAF1(40).

As previously described(20, 34, 41), we identified two antibodies that simultaneously bound to each target in its native state on flow cytometry beads, and validated target specificity with cell lysates lacking these targets (fig. S3 and table S3). Detergent optimization is critical to co-immunoprecipitation experiments, but with multiplex co-immunoprecipitations, one must select the best compromise detergent for the hundreds of potential binary interaction measurements(42). We compared digitonin, a detergent used in studies of TCR signaling because of its ability to maintain native TCR/CD3 complexes, with NP-40, a detergent used in studies of CAR signaling that is better than digitonin at solubilizing the CAR. We found a strong effect of detergent on detected protein networks; whereas many protein-protein interactions (indicated by “a_b,” where a and b represent the interacting proteins) were detected in samples treated with either detergent, others were better detected in samples treated with NP-40 (for example, CAR_ZAP70) or in samples treated with digitonin (for example, SLP76_LAT) (fig. S4). We used NP-40 in some experiments (Fig. 2) to ensure detection of CAR_ZAP70, whereas we used digitonin in the remaining experiments to maximize detection of the TCR signalosome. Finally, we optimized the co-immunoprecipitation procedure by varying the time of lysate-bead incubation (2 hours or overnight) and assessed the necessity of pre-clearing the lysate with flow cytometry beads to prevent nonspecific binding. We found that overnight incubation resulted in better detection of protein complexes, whereas pre-clearing was not necessary (fig. S5).

Activity-induced changes in protein interaction networks after TCR and CAR stimulation

To quantify acute changes in protein-protein interactions caused by CAR engagement, we stimulated four batches of bbζCAR T cells derived from the same donor with anti-CD3– or CD19-expressing K562 cells or with parental K562 cells (Fig. 2A). Weighted correlation network analysis(43) (CNA) of interaction intensity matrices identifies ”modules” of protein complexes that change in unison across multiple samples and experiments. Previous work demonstrated that interaction modules correlate with experimental stimuli more robustly than do individual interactions because groups of interactions changing in unison are less stochastic than any single interaction(44, 45). CNA identified a TCR Stimulation module whose behavior correlated with CD3 stimulation [correlation coefficient (CC) = 0.92] and also correlated to a lesser degree with CD3 and CD19 stimulation (CC=0.74) (Fig. 2B). The module contained 17 interactions that were also significantly different between unstimulated and anti-CD3–stimulated cells by a second, independent statistical test, “adaptive nonparametric test corrected for multiple comparisons” (ANC), which was designed specifically for QMI data (Fig. 2C) (20). The individual interaction that best

correlated with the eigenvector of the TCR Stimulation module was LCK_ZAP70 (Fig. 2D), which indicated activation of the CD3ζ-LCK-ZAP70 cascade that is typical of TCR signaling. Increased PI3K_LAT (Fig. 2E) and SLP76_LAT indicated that ZAP70 activation initiated the formation of a LAT-mediated signaling complex. In previous studies, PI3K_LAT was the complex most increased in abundance after pMHC-dependent stimulation of naïve, double-positive mouse thymocytes[14]. Furthermore, TRAF2_TRAF2, TAK1_TAK1, and TNIK_TNIK were also increased in abundance. Because proteins are unlikely to be synthesized de novo in 5 min, this increase in QMI detection may indicate changes in homo-oligomerization or in the accessibility of antibody epitopes and is suggestive of conformational changes in TRAF signaling complexes downstream of TCR-CD3 stimulation. Protein-protein interactions that significantly changed were represented by node-edge diagrams for CAR and mock T cells (Fig. 2, F and G). Although not identical due to biological noise and the stringency of the statistical analysis, these diagrams were consistent between CAR and mock T cells, indicating that CAR expression did not alter TCR-mediated signaling.

After CAR stimulation, three interactions in the “TCR Stimulation” module, LCK_CD3ζ, LCK_ZAP70, and PI3K_LAT, were significantly increased, demonstrating partial, although considerably weaker, activation of ZAP70-to-LAT signaling downstream of CAR ligation (Fig. 2, D and E). In addition, we identified a second module, which correlated with CAR expression (CC = 0.92), and, to a lesser extent, with CAR stimulation (CC = 0.56). The interaction whose behavior most strongly correlated with the behavior of this “CAR” module, CAR_CD3ζ, was strongly detected in unstimulated CARs, and was significantly reduced after stimulation (Fig. 2H). Note that the CD3ζ probe antibody detects a portion of CD3ζ that is included in the CAR construct(46), so this interaction may measure immunoprecipitation or multimerization of the CAR itself, or an interaction between the CAR and a native CD3ζ component, such as the CD3ζ “p21” protein that co-associates with second-generation CARs(47). CAR_ZAP70 (Fig. 2I), CAR_TRAF1, and TRAF1_CD3ζ increased after CAR ligation, and the abundances of TRAF2_TRAF2 and TAK1_TAK1 decreased, indicative of changes to their multimerization, binding partners, or antibody accessibility.

As with the MS data, we were surprised by the relatively weak activation of TCR signaling pathways by the CAR. To confirm that this weaker formation of protein complexes correlated with reduced phosphorylation of downstream targets, we performed Western blotting analysis to compare the total and phosphorylated amounts of ZAP70 ($pTyr^{319}$), LAT ($pTyr^{220}$), and PLC-γ1 ($pTyr^{783}$). Whereas CD3 stimulation resulted in statistically significant increases in all phosphorylation ratios, CD19 stimulation produced only small, nonsignificant changes (fig. S6), consistent with a previously published comparison of CD3 and BBζCAR stimulation(15). Overall, these data indicate the rapid formation of a CAR-ZAP70 signaling complex, which activates TCR-signalosome components to a lesser degree than does TCR-mediated signaling, and the simultaneous engagement of a TRAF signaling complex that is unique to the CAR.

Reconciling inconsistencies in the QMI and MS datasets

We expected interactions such as CAR_LCK or CAR_CD3 to increase, not decrease, after CD19 ligation, because signalosome activation is thought to involve the assembly of protein complexes. However, QMI queries protein complexes in the native state, so an apparent reduction in the extent of an interaction may reflect a true reduction in the measured co-association or an inability of a probe antibody to bind to a target decorated with activity-dependent interactions or ubiquitin chains. It may also reflect the CAR irreversibly binding to fixed target cells and being excluded from the soluble lysate. To discount this latter possibility, we repeated the experiment with unfixed target cells. Similarly to its response to fixed targets, the CAR showed increased apparent co-association with TRAF1 and ZAP70, but decreased co-association with CD3ζ, LCK, and TRAF2. PI3K_LAT was increased, whereas other CD3-responsive interactions were not significantly changed (fig. S7). We also performed coimmunoprecipitation Western blotting analysis of the CAR before and after stimulation with fixed targets and found equal amounts of CAR in the immunoprecipitates (fig. S8), suggesting a conformational explanation for the apparent reduction in CAR_CD3ζ. When Western blotting enabled detection of coimmunoprecipitated TRAF2 (which did not occur in all experiments), we found an increase in the amount of TRAF2 co-associated with the CAR (fig. S8A), consistent with the MS data (Fig. 1) and previous reports(48). These data reveal a consistent pattern of changes in CAR co-associations in experiments with fixed and unfixed targets and discount the hypothesis that the activated CAR is depleted from the lysate by binding to fixed targets.

Another potential caveat of coimmunoprecipitation experiments is that the interactions may form after lysis and may include proteins derived from the APCs. Isotope-labeled MS analysis showed that TRAF1, ZAP70, and PKCθ were 100% T cell–derived, whereas up to 66% of TRAF2 was APC-derived (table S1). To confirm that the observed CAR interactions occurred in T cells, we performed an APC-free platebound stimulation experiment (fig. S9). In response to anti-CD3/28, significant changes were observed in a “TCR stimulation” module in both mock-transduced and CAR T cells (fig. S9C), including PI3K_LAT (fig. S9E) and interactions containing GRAP2 and SLP-76, consistent with the formation of a TCR signalosome(20). Interactions in the “CAR” module (fig. S9D) included the complexes CAR_TRAF2, CAR_PKCΦ, CAR_ZAP70, and CAR_CD28, indicating that these complexes were present in the absence of APCs. However, interactions did not change significantly in the context of stimulation with plate-bound CD19, consistent with the lack of IL-2 expression, indicating that stimulation with plate-bound CD19 was unproductive (fig. S9H). These data support a model in which, after CD19 engagement, recruited protein complexes or ubiquitination events sterically hinder QMI probe antibodies, resulting in paradoxically reduced complex detection by QMI.

Effects of scFv on bbζCAR signaling complexes

Differences in the behaviors of CARs targeted to different antigens are well-established, and can be due to differences in tonic activation, the size or abundance of the protein target, or small differences in CAR design(49). In addition, batch-to-batch variations inherent to the manufacturing process may contribute to variable clinical responses(50). To quantify similarities and differences in CAR signaling due to batch vs. scFv target,

we generated four batches of CAR T cells from a single donor, two with an anti-CD19 scFv and two with an anti-EGFR“806” scFv(51), identical in structure except for the specificity-determining scFv. Cells were stimulated through the CAR with fixed K562 cells expressing CD19 or EGFR, and parental K562 cells were used as a control. Hierarchical clustering of the data matrices showed samples clustering first by stimulation, then by CAR type (anti-CD19 vs. anti-EGFR), and finally by batch (Fig. 3A). CNA identified two modules that correlated with CAR stimulation: a “TCR-like” module (CC = 0.62, $p = 4\times10^{-4}$) and a “CAR” module (CC= −0.64, $p = 1\times10^{-4}$) (Fig. 3B). The interaction most highly correlated with the behavior of the “TCR-like” module was PI3K_LAT (Fig. 3, C and D), followed by SLP76_LAT, indicating consistent formation of the LAT signalosome after CAR engagement. CAR_ZAP70 (increased, Fig. 3E), CAR_PKCΦ (decreased, Fig. 3F), and CAR_SHP2 were also members of the “TCR stimulation” module, suggesting that these interactions contribute to the formation of a TCR-like signalosome downstream of CAR ligation. The apparent abundance of CAR module interactions, including BIRC3_BIRC3 (Fig. 3G), TRAF1_BIRC3, and CAR_TRAF2 (Fig. 3H), decreased upon bbζCAR engagement, indicative of a rearrangement of TRAF signaling components that contribute to the orchestration of bbζCAR signaling, as discussed earlier. These data define a core set of protein complexes, organized into two modules, that mediate bbζCAR signaling in different CAR constructs (Fig. 3J).

Whereas we were able to detect interactions that changed in all batches, there were also clear differences in the extents of interactions between the four batches of CAR T cells due to first target type, then manufacturing run. Uncontrollable differences between CAR production batches may contribute to clinical CAR performance, one indicator of which was IL-2 secretion after overnight incubation with target cells. The average amount of IL-2 secreted by each batch (measured for each experimental replicate and then averaged) correlated with the average MFI of CAR_ZAP70 after CD19 exposure (Fig. 3I), with the batches showing the strongest signalosome activation also showing the greatest IL-2 production. These data suggest that batch-specific signalosome activation may predict batch-specific CAR performance and prompted us to explore this relationship among different donors.

Donor-dependent differences in CAR signaling predict IL-2 production

All of the previous experiments were performed with CAR T cells manufactured from single donors to eliminate genotype-dependent variations. To investigate individual variations, we made four batches of anti-CD19 bbζCAR from four donors and stimulated them with fixed K562 target cells expressing anti-CD3 or CD19. CNA again identified a TCR-like module that correlated with both anti-CD3 stimulation (CC = −0.91, $p = 9 \times 10^{-9}$) and CD3 or CD19 stimulation (CC = −0.73, $p = 6 \times 10^{-5}$), and a CAR module that correlated with CAR expression (CC = 0.82, $p = 7 \times 10^{-7}$) (Fig. 4, A and B). The TCR module contained interactions representing the TCR complex, including TCR_CD3ζ (Fig. 4C), which was not detected in experiments in which cells were lysed in NP-40 (Fig. 2 and fig. S3), as well as PI3K_SLP76 and PI3K_LAT (Fig. 4D), representing TCR signalosome formation. The CAR module contained CAR- and TRAF-containing interacting partners, including CAR_ZAP70 and CAR_TRAF2 (Fig. 4, E and F), which was reduced in its apparent abundance after

CAR stimulation. The intensity of CAR_ZAP70 (Fig. 4G) correlated with IL-2 secretion measured in overnight cultures, again indicating that signalosome formation may predict in vitro performance. Node-edge diagrams illustrated similar signalosome formation in mock and CAR T cells downstream of CD3 stimulation (Fig. 4, H to J), which shared PI3K-LAT-SLP76 signalosome components with CAR stimulation (Fig. 4I). These data demonstrate that signalosome formation downstream of TCR and CAR is qualitatively similar, but quantitatively different among different donors. These intensity differences correlated with a functional readout of CAR activity.

Discussion

Activity-dependent protein-protein interactions are the key mediators of intracellular signaling events but are difficult to identify and monitor at scale. We used MS and QMI to detect two modules of coordinated protein-protein interactions that changed their pattern of co-associations after CAR activation: a TCR-like module and a CAR-TRAF module (Fig 5). TCR activation is initiated by the kinase LCK, some of which is bound to a CXCP motif on the coreceptors CD4 or CD8a(11) and brought into physical proximity with the TCR when these coreceptors interact with pMHC. Free, membrane-tethered LCK, not bound to coreceptor, may also play a role in basal TCR phosphorylation and activation(52), as may LCK bound to the TCR through an interaction involving the CD3ε basic residue rich sequence (BRS) motif(53). The CAR does not engage CD4 or CD8, nor does it contain a CD3ε motif, so the origin of activating LCK is assumed to be the free LCK pool, which has increased kinase activity than that of the bound pool(52) but may not form a stable protein complex with the CAR. Irrespective of the source of LCK, the next step in both TCR and CAR activation is the recruitment of ZAP70 to LCK-phosphorylated ITAMs and its subsequent phosphorylation by LCK, leading to ZAP70 activation. In the TCR system, LCK binds simultaneously to TCR-bound, activated ZAP70 and to the scaffolding adaptor protein LAT, increasing the efficiency of the signaling cascade(54). Phosphorylated LAT assembles a signalosome consisting of GRAP2, SLP-76, PLC-γ1, PI3K, and many other signaling molecules to collectively amplify TCR signals and initiate calcium (Ca^{2+}) signaling, MAPK activation, and actin polymerization(11). Consistent with this model, after stimulation of the TCR with OKT3, QMI detected the increased abundances of CD3_LCK, LCK_ZAP70, LAT_SLP76, PI3K_LAT, SLP76_PLCg, and others in both CAR and mock T cells. After CAR stimulation, PI3K_LAT and SLP76_LAT were detected, but their magnitude of activation was lower compared to that after TCR stimulation, and the other interactions were not detected. Indeed, there were few other canonical TCR-associated proteins that associated with the CAR after stimulation. Moreover, phosphorylated proteins that increased in abundance after TCR stimulation did not increase after CAR stimulation, and “T cell signaling” was not an enriched GO or KEGG pathway in the MS data. These data are consistent with previous studies of CAR T cells showing less efficient LCK engagement and ZAP70 mobility(14) and less ZAP70-mediated phosphorylation of downstream adaptors, such as PLC-γ and LAT(16). The QMI assay can acutely measure this inefficient, TCR-associated signalosome formation after CAR activation, offering a platform to monitor CAR performance and screen for improved CAR designs.

A second signaling module identified by MS and QMI encompasses TRAF signaling, consisting of TRAF1/2/D1, BIRC2/3, and TAB1/2. TRAF signaling mediates endogenous 4–1BB signaling, and the importance of TRAF1(18) and TRAF2(48), which lead to both canonical and noncanonical NF-κB activation(19) downstream of bbζCAR activation, has been established. By QMI, CAR_TRAF2 and multiple TRAF-containing interactions appeared to be reduced by CAR stimulation, but IP-MS and IP-Western blots performed by us and others(48) showed increases in the amount of CAR_TRAF2. This discrepancy may highlight a known caveat of probing protein complexes in the native state: antibody accessibility may be reduced as signaling complexes form. Together, our data support a model (Fig. 5) in which, before CAR ligation, CARs are associated with trimers consisting largely of TRAF2. After CAR activation, the ratio of TRAF1/2 bound to the CAR changed, and although the absolute amount of TRAF2 co-associated with the CAR increased (as assessed by Western blotting and MS analyses), the accessibility of QMI probe antibodies to bind TRAF2 decreased. Because the QMI probe antibody binds to the TRAF2 zinc-finger domain adjacent to the RING domain, which is the site of binding-partner recruitment and ubiquitin conjugation after TRAF activation(55, 56), these data are consistent with an activation event. Because the ratio of TRAF1 to TRAF2 found in the T cell can alter the binding affinity of effector molecules such as BIRC3(57), future studies of TRAF abundance in CAR T cell products, including autoimmunity-associated SNPs that affect TRAF1 abundance, seem warranted.

Many open questions remain about how CAR binding to CD19 may stimulate TRAF signaling, particularly because TRAF2 is predominantly a trimer at physiological concentrations(58), and natural TRAF ligands are trimeric (17, 56), whereas the BBζ CAR is a dimer in vivo and does not have an obvious trimerization mechanism. TRAF2 binds to a linear, 10-amino-acid consensus sequence (P/S/A/T)X(Q/E)E(59), and the CAR construct contains two copies of this sequence. The sites are too close to each other to enable simultaneous binding of two TRAF molecules to a single CAR(59), but having two sites per CAR (and four sites per CAR dimer) may overcome the relatively weak affinity of the interaction (~30 to 60 μM) by increasing its avidity(60). TRAFs are thought to form a hexagonal lattice structure both at rest and after stimulation, with trimers at each vertex connected by dimeric linkages of TRAF2 N-terminal RING domains or of bound BIRC2/3 (17, 56). Perhaps the dimeric CAR can similarly serve as a linker to induce or stabilize the lattice, but the mechanism through which the binding of CD19 to the scFv of the CAR is transmitted to the TRAF system remains unclear. Future work to reconcile whether this structure serves to amplify CAR signaling by acting as a scaffold or to reduce tonic signaling by spacing CAR dimers apart on the membrane is needed to provide structural insights into the mechanisms of BB costimulation.

The third major signaling component identified by MS was cytoskeletal motility; proteins linked to early endocytic vesicle formation (FLOT1/2), microtubule spindle formation (KIFs, MYO), and T cell migration in response to stimulation (DOCK8) were identified. Activated CARs form nonclassical immune synapses(61), but, unlike TCRs, they do not rely on LAT to cluster(62). Perhaps the ability of a CAR to engage cytoskeletal elements enables it to bypass LAT and form nonclassical immune synapses. Alternatively, these

data could reflect the sequestration of activated CARs into endosomal compartments for degradation(48).

Other signaling molecules were also identified by MS or QMI that do not fit cleanly into either the TCR or TRAF modules. PKCβ (identified by MS) and PKCθ (identified by MS and QMI) are both members of the PKC family and are activated by DAG and Ca^{2+}. PCKθ plays a major role in NF-κB activation during T cell activation(11), and PCKβ directly phosphorylates CARD11/CARMA1, promoting the recruitment of the BCL-10/MALT1 complex and TAK1 to activate NF-κB(63). UBASH3A interacts with CBL-B, CD3ζ and ZAP70 in stimulated T cells(24) and may contribute to CAR endocytosis and degradation after activation. Finally, the phosphatase SHP2, which was already a member of the QMI TCR panel(20), associated with the CAR, an interaction that was reduced after stimulation. A complex containing Themis and SHP1 co-associates with bbζCARs with a requirement for a 10-amino acid region that overlaps with one of two TRAF2-binding sites(64), and SHP2 may bind in a similar manner. Although the specific interactors we identified require further investigation, it is striking that the CAR signaling network is reminiscent of a human T cell signaling network based on a nonbiased CRISPR screen, which identified both classical TCR signaling molecules and NF-κB pathway regulators as being critical to T cell signaling(35).

Whereas we sought to define a bbζCAR signalosome common to all bbζCARs, we observed moderate batch- and CAR-dependent variability. This variability has important clinical implications, because batch-to-batch differences in efficacy and toxicity profiles complicate treatment outcomes. We found that CAR_ZAP70 activation at 5 min corelated with the amount of IL-2 produced in an overnight assay, which confirms that signalosome activation affects functional outcomes. More complex clinical outcomes, such as CAR persistence or survival, could potentially also correlate with signalosome measures unique to each batch. For example, differing ratios of the abundance of TRAF1 to TRAF2, the former of which is only expressed after T cell activation(65), could affect CAR performance. SNPs in *TRAF1* affect the amount of TRAF1 production and contribute to the risk of rheumatic disease(40), and the abundance of TRAF1 can influence the activation of canonical vs. noncanonical NF-κB activation downstream of 4–1BB stimulation(66). Multiplexed measurement of protein signaling networks in CAR T cells combined with detailed analysis of patient outcomes could enable the identification of protein network features that predict an optimal outcome and facilitate the rational design of CAR features or the engineering of intracellular environments that lead to optimal functional performance.

Materials and Methods

Cell culture

CAR T cells and MOCK T cells were prepared using an 8- to 12-day expansion protocol adapted from clinical production practices. Peripheral blood mononuclear cells (PBMCs) were harvested from Leukocyte Reduction System (LRS) Cones provided by STEMCELL Technologies and cryopreserved. Cells were thawed into XVIVO medium (Lonza) supplemented with IL-2 (4.6 ng/ml), IL-7 (5 ng/ml), IL-15 (0.5 ng/ml), and IL-21 (1 ng/ml; Miltenyi Biotec) at a density of 1×10^6 cells/ml and activated with Human

T-Activator CD3/CD28 Dynabeads (ThermoFisher). On day 1, cells were concentrated to a density of 4×10^6/ml and then either transduced with lentiviral vectors encoding CAR constructs at an MOI of 2 with protamine sulfate (25 μg/ml, Sigma-Aldrich) or vector-less medium with protamine sulfate (25 μg/ml). Twenty-four hours later, the cells were moved to GREX 24-well plates (Wilson Wolf) for further expansion at 1×10^6/ml in XVIVO medium with cytokines until Dynabeads were removed by magnet on day 7. Cells were propagated until they were harvested on days 8 to 12. Human Jurkat cells (ATCC clone E6–1, #TIB-152), CARKats (Jurkat cells stably transduced with CD19CAR-encoding virus), parental Human K562 cells (ATCC #CCL-243), and K562s expressing either CD19 or OKT3 were cultivated in 10% heat-inactivated FBS, 1% glutaraldehyde, 1% penicillin-streptomycin, 1% Hepes, and RPMI 1640 in 175-ml non-TC treated flasks. For heavy isotope–labeling of K562 cells, cells were labeled with heavy Lysine and Arginine with a SILAC protein quantitation kit (ThermoFisher Cat # 1863109) according to the manufacturer's instructions, and labeling was confirmed by MS.

Target cell fixation

APCs for the stimulation of primary cells were washed twice in ice-cold PBS and then fixed for 30 s in 4 ml of PBS with 0.1% glutaraldehyde (Sigma) on ice. This was immediately followed by quenching with 16 ml of 200 mM glycine. Cells were washed twice more in ice-cold PBS, counted, and mixed with CAR T cells for stimulation.

Cell stimulation

For plate-bound activation of cells, CD19 recombinant protein (R&D Systems) or anti-CD3 (clone OKT3, Biolegend) with anti-CD28 (clone CD28.2 Biolegend) antibodies were annealed to the wells of 6-well TC coated plates overnight with PBS added to the wells as a control. CAR or Mock T cells (3×10^6 cells) were washed twice in ice-cold PBS, added to plates, and then subjected to a 1-min centrifugation at 300*g* to bring the cells into contact with the plate-bound protein. Plates were placed in a 37°C water bath for 5 min, which was followed by immediate lysis in 1% digitonin lysis buffer on ice. For activation involving K562 cell targets, CAR T and target cells (fixed or unfixed) were washed twice in ice-cold PBS and then combined at a 1:1 ratio and mixed. Cells were spun at 300*g* for 5 min at 4°C, the PBS was removed, and the pellet was agitated by wash-boarding the tube across an uneven surface. Cell pellets were stimulated by immersing the tubes in a 37°C water bath for 5 min, which was followed freezing in liquid nitrogen. Cell pellets were stored at −80°C until required for further processing.

Cell lysis

Frozen cell pellets were resuspended in 250 to 500 μl of lysis buffer [1% Digitonin or NP-40, 1x phosphatase inhibitor cocktail (Sigma), 1x protease inhibitor cocktail (Sigma), 1 mM sodium orthovanadate (Sigma) and 1 mM sodium fluoride (Sigma) in 50 mM Tris, 150 mM NaCl, (pH 7.4)]. Lysates were incubated on ice for 15 min and then centrifuged at 13,000*g* for 10 min at 4°C. Supernatants were harvested and used for the immunoprecipitation of protein targets.

Coimmunoprecipitation for MS

Cryopreserved CAR T cells produced from heathy donors in the Seattle Children's GMP production facility were thawed and cultured overnight in XVIVO medium (Lonza) supplemented with IL-2 (4.6 ng/ml), IL-7 (5 ng/ml), IL-15 (0.5 ng/ml), and IL-21 (1 ng/ml). For the first experiment, on the following day, the cells were mixed 1:1 with fixed target cells (as described earlier) and either warmed for 5 min at 37°C to enable signaling to proceed or maintained on ice to control for scFv-CD19 binding without signaling. For the second experiment, on the following day, the cells were maintained at 37°C while they were mixed 1:1 with fixed, heavy isotope–labeled K562 parental cells or K562-CD19 cells, and then incubated at 37°C for 5 min before undergoing lysis in 1% NP-40 lysis buffer. Protein G magnetic beads (NEB) were incubated with anti-2A (experiment 1, clone 3H4, Novus) or anti-FM63 (experiment 2, clone REA1298, Miltenyi biotech) for 40 min at room temperature with agitation, which was followed by cross-linking of antibody to the beads by incubation in 25 mM DMP for 45 min with agitation at room temperature. The cross-linking reaction was quenched with 50 mM Tris-HCl. Cell lysates were incubated overnight with antibody–protein G beads, washed twice in lysis buffer, washed twice in lysis buffer without detergent, and proteins were eluted in 200 mM glycine (pH 2) (experiment 1) or eluted by on-bead trypsin digestion (experiment 2). For experiment 1, eluted proteins were precipitated with methanol-chloroform, and the pellets were sent for processing and MS analysis.

Coimmunoprecipitation for Western blotting

Protein G beads covalently bound and cross-linked to 2A antibodies for coimmunoprecipitations to be analyzed by Western blotting were prepared according to MS sample preparation with the addition of a final elution of excess uncrosslinked antibody with 200 mM glycine (pH 2). Eluted proteins were precipitated in acetone. Additionally, immunoprecipitations for Western blotting analysis were performed on cell lysates derived from APCs mixed with CAR and Mock Transduced primary T cells from LRS Cones (STEMCELL).

MS analysis

Protein pellets were resuspended in 20 μl of 8 M urea in 100 mM ammonium bicarbonate and vortexed thoroughly. Protein disulfide bonds were reduced by the addition of tris (2-carboxyethyl) phosphine (TCEP) to a final concentration of 20 mM and incubated at room temperature for 20 min. Cysteines were alkylated by the addition of 2-chloroacetamide to a final concentration of 20 mM and incubation at room temperature for 30 min. Proteolytic digestion was initiated by the addition of 250 ng of endoproteinase Lys-C (Promega) and incubation at room temperature for 2 hours. The proteolytic digestion was continued by the addition of 500 ng of trypsin (Promega) and incubation overnight at 37°C with gentle shaking. Digestions were stopped by the addition of trifluoroacetic acid (TFA) to a final concentration of 0.1%. The resulting peptide samples were desalted on a C18 Ultra-micro Spin Column (Harvard Apparatus) using 70% acetonitrile in 0.1% TFA and taken to dryness by vacuum centrifugation. Dried samples were brought up in 20 μl of 2% acetonitrile in 0.1% formic acid, and 5 μl was analyzed by LC/ESI MS/MS with a

ThermoFisher Scientific Easy1000 nLC coupled to an Orbitrap Fusion mass spectrometer. In-line de-salting was accomplished with a reversed-phase trap column (100 μm × 20 mm) packed with Magic C_{18}AQ (5-μm, 200Å resin; Michrom Bioresources), followed by peptide separations on a reversed-phase column (75 μm × 270 mm) packed with ReproSil-Pur C_{18}AQ (3-μm, 120Å resin; Dr. Maisch) directly mounted on the electrospray ion source. Chromatographic separation was performed by adjusting the elution gradient from 5 to 28% B (80% acetonitrile with 20% water and 0.1% formic acid) for 90 min, 28 to 50% B for 10 min, holding at 50% B for 3 min, 50 to 95% B for 2 min, and holding at 95% B for 1 min. A flow rate of 300 nl/min was used for chromatographic separations and the temperature of the chromatographic column was maintained at 40°C. A spray voltage of 2200 V was applied to the electrospray tip while the Orbitrap Eclipse instrument was operated in the data-dependent mode. MS survey scans were in the Orbitrap (AGC target value: 5E5; resolution: 120,000; and max injection time: 50 ms) using a scan range of 400 to 1500 m/z and a 3-s cycle time. MS/MS spectra were acquired in the linear ion trap (AGC target value: 1×10^4; rapid scan rate; and max injection time: 45 ms) with an isolation window of 1.6 and using higher-energy, collision-induced dissociation (HCD) activation with a collision energy of 27%. The dynamic exclusion duration was set to 20 s. Protein database searching and label-free quantification (LFQ) were performed with ThermoFisher Scientific Proteome Discoverer v2.4. The data were searched against a Uniprot human database (UP000005640; downloaded 12/01/2019) that included common contaminants (cRAP; Global Proteome Machine). Search settings included the proteolytic enzyme set to trypsin, maximum missed cleavages set to 2, precursor ion tolerance set to 10 ppm, and the fragment ion tolerance set to 0.6 Da. Dynamic modifications were set to oxidation on methionine (+15.995 Da), phosphorylation on serine and threonine (+79.966), acetylation of the protein N terminus (+42.011 Da), methionine loss at the protein N terminus (−131.040 Da), and methionine loss and acetylation of the protein N terminus (−89.030 Da). A static modification of carbamidomethylation of cysteine (+57.021 Da) was used. Sequest HT was used for protein database searching, and Percolator was used for peptide validation. Peptide to spectrum matches (PSMs) were filtered to a 1% FDR, and the resulting proteins were further filtered to a 1% FDR. LFQ analysis was performed with the Precursor Ion Quantifier node using the default settings. Normalization was performed with the total peptide amount setting.

Screening QMI antibodies with IP-FCM

This procedure was performed as described previously(67). CML Beads (CML Latex Microspheres) were activated with EDAC [1-ethyl-3-(3-dimethylaminopropyl) carbodiimide HCL] and then coupled to 50 μl of antibody at 0.5 mg/ml for 2 hours at room temperature with agitation at 1400 rpm. Probe antibodies were biotinylated at a 50-fold molar excess with EZ-link Sulfo-NHS-Biotin (Thermo). Coupled CML beads were added to the lysates of frozen cell pellets at equal bead to protein quantity ratios across conditions and then incubated at 4°C overnight with rotation. Beads and any bound protein complexes were then washed three times in Fly-P buffer [100 mM NaCl, 50 mM Tris, 1% bovine serum albumin, 0.01% sodium zzide, (pH 7.4)] before being distributed across a 96-well plate twice for every biotinylated probe antibody to be used. Probes were then added at a final concentration of 2.5 μg/ml, and the plate was incubated with agitation at 600 rpm for 1 hour at 4°C. The samples were then washed twice in Fly-P buffer, which was followed

by incubation in streptavidin-phycoerythrin (PE, 10 μg/ml, Biolegend) for 30 min. After three washes in Fly-P buffer, the CML beads were analyzed for PE fluorescence on a flow cytometer (Novocyte). Data consisted of MFI values and bead distributions.

QMI

QMI experiments were performed as described previously(20, 34). All experiments and procedures were performed at 4°C or on ice, starting with the preparation of a master mix of an equal number of each antibody-coupled Luminex bead used for the immunoprecipitations. Equal amounts of bead master mix were distributed to cell lysates, whose protein concentrations were normalized by BCA assay. Immunoprecipitations of protein complexes were performed overnight with rotation, and then samples were washed twice in Fly-P buffer and beads were distributed across a 96-well plate at two wells per detection antibody. Biotinylated or PE-conjugated detection antibodies diluted to a final concentration of 2.5 μg/ml were added to the plate for 1 hour with shaking at 600 rpm. Details about immunoprecipitating and detection antibodies can be found in table S2. After three washes in Fly-P buffer with the Bio-Plex Pro II magnetic plate washer, microbeads and captured protein complexes stained with detection antibody were incubated in streptavidin-PE or Fly-P buffer for 30 min, then washed again as described earlier and resuspended in 120 μl of Fly-P buffer. Fluorescence was analyzed and data acquired through a customized, refrigerated Bio-Plex 200 using Bio-plex Manager software (v.6.2). XML formatted data files were exported for further analysis.

QMI data analysis

A detailed video protocol and source code for QMI data analysis were previously published(34), including statistical code run in MatLab (ANC) or R (CNA). Briefly, for CNA, data were normalized with the ComBAT function(68). Interactions were organized into modules based on correlated behavior across experimental conditions and replicates with the WGCNA package(43), and modules were then correlated with experimental variables. Interactions that were significantly ($P < 0.05$) and strongly (module membership < 0.7) correlated to a module that was itself significantly correlated to an experimental variable were considered “CNA-significant.” Modules that correlated with CD3 stimulation and contained PI3K_LAT were renamed “TCR simulation,” and modules that correlated with CAR abundance and contained CAR-containing interactions were renamed “CAR,” to highlight the fact that whereas the specific interactions that constituted each module varied by experiment, the same overall patterns were observed between experiments, similar to previous reports about RNA abundance(69). Meanwhile, for ANC statistical testing (Adaptive, Nonparametric test Corrected for multiple comparisons), individual interactions were compared for each experimental N between the stimulated group and the control group by nonparametric Kolomogrov-Schmirnov statistics corrected to maintain a type 1 error rate of 0.05 and corrected for multiple comparisons by Bonferroni correction. For the equations, see the study by Smith et al. (20). Only interactions that were deemed significant by both ANC and CNA are displayed in the heatmaps and node-edge diagrams, which were generated in R and Cytoscape, respectively.

Western blotting

All Western blotting experiments consisted of proteins denatured in SDS sample buffer (4x, Bio-rad) with 10% (v/v) beta-mercaptoethanol and loaded onto 10% acrylamide gels. Gels were transferred onto polyvinylidene difluoride (Millipore) membranes and then blocked in 4% milk TBST [0.05 M Tris, 0.15 M NaCl, (pH 7.2), 0.1% (v/v) Tween-20] for 60 min at room temperature with gentle rocking. Primary antibodies were applied overnight at 4°C in 4% milk. The following primary antibodies were used, all at a 1:1000 volumetric dilution: anti-2A (3H4, Novus), anti-TRAF2 (F-2, Santa Cruz), anti-ZAP70 (D9H10, Novus), anti-TAK1 (28H25L68, Thermo), anti-phospho-ZAP70 (65E4, Cell Signaling), anti-phospho-LAT (cat# 3584 Cell Signaling), anti-LAT (Clone 661002, Cell Signaling), anti-phospho-PLCγ1 (D25A9, Cell Signaling), and anti-PLCγ1 (D9H10, Cell Signaling). Blots were incubated with species-specific, horseradish peroxidase (HRP)–conjugated antibodies and then imaged with SuperSignal West Femto substrate (Thermofisher) on a Protein Simple imaging system.

IL-2 ELISA cytokine release assay

Effector and target cells were combined at various ratios in XVIVO medium without cytokines at a density of 1×10^6 effector cells/ml and incubated overnight at 37°C, 5% CO_2 in 96-well non-TC plates. Cells were then centrifuged at 300*g* for 5 min and supernatants were frozen at −80 C. The IL-2 concentration in the harvested supernatant was then analyzed with a Human IL-2 ELISA Max Kit (BioLegend) according to the manufacturer's instructions. All cell effector activations were performed in four separate replicates and analyzed as separate samples. A SpectraMax i3x plate reader was used for spectrometry and data generation.

Statistical analysis

MS data and QMI data were analyzed as described earlier. For all other data, Prism GraphPad software was used to make comparisons between two groups with student's T-tests, comparisons among multiple groups with one-way ANOVA followed by Sidak's multiple-comparison-corrected post-hoc testing, and linear regressions using the simple linear regression function.

Supplementary Material

Refer to Web version on PubMed Central for supplementary material.

Acknowledgments:

We thank B. K. Reed, J. Gust, A. Faino, and the entire SEPS lab for helpful discussions and technical assistance. We gratefully acknowledge the following individuals for providing cell lines or reagents: S. Cramer, J. L. Maiers, C. Mayr, H. Wajant, T. H. Watts, and N. Bidère. We also thank M. A. Jackson for providing protocols and CAR constructs and L. Jones for assistance with MS data collection.

Funding:

This work was funded by National Institutes of Health grant R01CA240985 (to S.E.P.S.). The Proteomics & Metabolomics Shared Resource of the Fred Hutch/University of Washington Cancer Consortium is funded by NCI

grant P30CA015704, and the Orbitrap Fusion mass spectrometer used in this research was funded by the M. J. Murdock Charitable Trust.

Data and materials availability:

Raw MS files were uploaded to MassIVE under accession number MSV000092691. All other data needed to evaluate the conclusions in the paper are present in the paper or the Supplementary Materials.

References and Notes

1. Wu L, Wei Q, Brzostek J, Gascoigne NRJ, Signaling from T cell receptors (TCRs) and chimeric antigen receptors (CARs) on T cells. Cell. Mol. Immunol. 17, 600–612 (2020). [PubMed: 32451454]
2. Sadelain M, Rivière I, Riddell S, Therapeutic T cell engineering. Nature 545, 423–431 (2017). [PubMed: 28541315]
3. Neelapu SS, Locke FL, Bartlett NL, Lekakis LJ, Miklos DB, Jacobson CA, Braunschweig I, Oluwole OO, Siddiqi T, Lin Y, Timmerman JM, Stiff PJ, Friedberg JW, Flinn IW, Goy A, Hill BT, Smith MR, Deol A, Farooq U, McSweeney P, Munoz J, Avivi I, Castro JE, Westin JR, Chavez JC, Ghobadi A, Komanduri KV, Levy R, Jacobsen ED, Witzig TE, Reagan P, Bot A, Rossi J, Navale L, Jiang Y, Aycock J, Elias M, Chang D, Wiezorek J, Go WY, Axicabtagene Ciloleucel CAR T-Cell Therapy in Refractory Large B-Cell Lymphoma. N. Engl. J. Med. 377, 2531–2544 (2017). [PubMed: 29226797]
4. Jaklevic MC, CAR-T Therapy Is Approved for Non-Hodgkin Lymphoma. JAMA 325, 1032 (2021).
5. Maude SL, Laetsch TW, Buechner J, Rives S, Boyer M, Bittencourt H, Bader P, Verneris MR, Stefanski HE, Myers GD, Qayed M, De Moerloose B, Hiramatsu H, Schlis K, Davis KL, Martin PL, Nemecek ER, Yanik GA, Peters C, Baruchel A, Boissel N, Mechinaud F, Balduzzi A, Krueger J, June CH, Levine BL, Wood P, Taran T, Leung M, Mueller KT, Zhang Y, Sen K, Lebwohl D, Pulsipher MA, Grupp SA, Tisagenlecleucel in Children and Young Adults with B-Cell Lymphoblastic Leukemia. N. Engl. J. Med. 378, 439–448 (2018). [PubMed: 29385370]
6. Frey NV, Approval of brexucabtagene autoleucel for adults with relapsed and refractory acute lymphocytic leukemia. Blood, doi: 10.1182/blood.2021014892 (2022).
7. Gardner RA, Finney O, Annesley C, Brakke H, Summers C, Leger K, Bleakley M, Brown C, Mgebroff S, Kelly-Spratt KS, Hoglund V, Lindgren C, Oron AP, Li D, Riddell SR, Park JR, Jensen MC, Intent-to-treat leukemia remission by CD19 CAR T cells of defined formulation and dose in children and young adults. Blood 129, 3322–3331 (2017). [PubMed: 28408462]
8. Martinez M, Moon EK, CAR T Cells for Solid Tumors: New Strategies for Finding, Infiltrating, and Surviving in the Tumor Microenvironment. Front. Immunol. 10, 128 (2019). [PubMed: 30804938]
9. Gust J, Ponce R, Liles WC, Garden GA, Turtle CJ, Cytokines in CAR T Cell-Associated Neurotoxicity. Front. Immunol. 11, 577027 (2020). [PubMed: 33391257]
10. Schrum AG, Gil D, Robustness and Specificity in Signal Transduction via Physiologic Protein Interaction Networks. Clin. Exp. Pharmacol. 2, S3.001 (2012).
11. Shah K, Al-Haidari A, Sun J, Kazi JU, T cell receptor (TCR) signaling in health and disease. Signal Transduct. Target. Ther. 6, 1–26 (2021). [PubMed: 33384407]
12. de la Cruz J, Kruger T, Parks CA, Silge RL, van Oers NSC, Luescher IF, Schrum AG, Gil D, Basal and antigen-induced exposure of the proline-rich sequence in CD3ε. J. Immunol. Baltim. Md 1950 186, 2282–2290 (2011).
13. Neier SC, Ferrer A, Wilton KM, Smith SEP, Kelcher AMH, Pavelko KD, Canfield JM, Davis TR, Stiles RJ, Chen Z, McCluskey J, Burrows SR, Rossjohn J, Hebrink DM, Carmona EM, Limper AH, Kappes DJ, Wettstein PJ, Johnson AJ, Pease LR, Daniels MA, Neuhauser C, Gil D, Schrum AG, The early proximal αβ TCR signalosome specifies thymic selection outcome through a quantitative protein interaction network. Sci. Immunol. 4 (2019).

14. Gudipati V, Rydzek J, Doel-Perez I, Gonçalves VDR, Scharf L, Königsberger S, Lobner E, Kunert R, Einsele H, Stockinger H, Hudecek M, Huppa JB, Inefficient CAR-proximal signaling blunts antigen sensitivity. Nat. Immunol. 21, 848–856 (2020). [PubMed: 32632291]
15. Salter AI, Ivey RG, Kennedy JJ, Voillet V, Rajan A, Alderman EJ, Voytovich UJ, Lin C, Sommermeyer D, Liu L, Whiteaker JR, Gottardo R, Paulovich AG, Riddell SR, Phosphoproteomic analysis of chimeric antigen receptor signaling reveals kinetic and quantitative differences that affect cell function. Sci. Signal. 11, eaat6753 (2018). [PubMed: 30131370]
16. Salter AI, Rajan A, Kennedy JJ, Ivey RG, Shelby SA, Leung I, Templeton ML, Muhunthan V, Voillet V, Sommermeyer D, Whiteaker JR, Gottardo R, Veatch SL, Paulovich AG, Riddell SR, Comparative analysis of TCR and CAR signaling informs CAR designs with superior antigen sensitivity and in vivo function. Sci. Signal. 14, eabe2606 (2021). [PubMed: 34429382]
17. Zapata JM, Perez-Chacon G, Carr-Baena P, Martinez-Forero I, Azpilikueta A, Otano I, Melero I, CD137 (4–1BB) Signalosome: Complexity Is a Matter of TRAFs. Front. Immunol. 9 (2018).
18. Li G, Boucher JC, Kotani H, Park K, Zhang Y, Shrestha B, Wang X, Guan L, Beatty N, Abate-Daga D, Davila ML, 4–1BB enhancement of CAR T function requires NF-κB and TRAFs. JCI Insight 3, 121322 (2018). [PubMed: 30232281]
19. Philipson BI, O'Connor RS, May MJ, June CH, Albelda SM, Milone MC, 4–1BB costimulation promotes CAR T cell survival through noncanonical NF-κB signaling. Sci. Signal. 13, eaay8248 (2020). [PubMed: 32234960]
20. Smith SEP, Neier SC, Reed BK, Davis TR, Sinnwell JP, Eckel-Passow JE, Sciallis GF, Wieland CN, Torgerson RR, Gil D, Neuhauser C, Schrum AG, Multiplex matrix network analysis of protein complexes in the human TCR signalosome. Sci. Signal. 9, rs7 (2016). [PubMed: 27485017]
21. Elazar A, Chandler NJ, Davey AS, Weinstein JY, Nguyen JV, Trenker R, Cross RS, Jenkins MR, Call MJ, Call ME, Fleishman SJ, De novo-designed transmembrane domains tune engineered receptor functions. eLife 11, e75660 (2022). [PubMed: 35506657]
22. Mellacheruvu D, Wright Z, Couzens AL, Lambert J-P, St-Denis NA, Li T, Miteva YV, Hauri S, Sardiu ME, Low TY, Halim VA, Bagshaw RD, Hubner NC, Al-Hakim A, Bouchard A, Faubert D, Fermin D, Dunham WH, Goudreault M, Lin Z-Y, Badillo BG, Pawson T, Durocher D, Coulombe B, Aebersold R, Superti-Furga G, Colinge J, Heck AJR, Choi H, Gstaiger M, Mohammed S, Cristea IM, Bennett KL, Washburn MP, Raught B, Ewing RM, Gingras A-C, Nesvizhskii AI, The CRAPome: a contaminant repository for affinity purification-mass spectrometry data. Nat. Methods 10, 730–736 (2013). [PubMed: 23921808]
23. Shinohara H, Yasuda T, Aiba Y, Sanjo H, Hamadate M, Watarai H, Sakurai H, Kurosaki T, PKC beta regulates BCR-mediated IKK activation by facilitating the interaction between TAK1 and CARMA1. J. Exp. Med. 202, 1423–1431 (2005). [PubMed: 16301747]
24. Ge Y, Paisie TK, Chen S, Concannon P, UBASH3A Regulates the Synthesis and Dynamics of TCR–CD3 Complexes. J. Immunol. 203, 2827–2836 (2019). [PubMed: 31659016]
25. Matson CA, Choi S, Livak F, Zhao B, Mitra A, Love PE, Singh NJ, CD5 dynamically calibrates basal NF-κB signaling in T cells during thymic development and peripheral activation. Proc. Natl. Acad. Sci. 117, 14342–14353 (2020). [PubMed: 32513716]
26. Voisinne G, Gonzalez de Peredo A, Roncagalli R, CD5, an Undercover Regulator of TCR Signaling. Front. Immunol. 9 (2018).
27. Föger N, Marhaba R, Zöller M, CD44 supports T cell proliferation and apoptosis by apposition of protein kinases. Eur. J. Immunol. 30, 2888–2899 (2000). [PubMed: 11069071]
28. Ji Q, Salomon AR, Wide-Scale Quantitative Phosphoproteomic Analysis Reveals That Cold Treatment of T Cells Closely Mimics Soluble Antibody Stimulation. J. Proteome Res. 14, 2082–2089 (2015). [PubMed: 25839225]
29. Conner SH, Kular G, Peggie M, Shepherd S, Schüttelkopf AW, Cohen P, Van Aalten DMF, TAK1-binding protein 1 is a pseudophosphatase. Biochem. J. 399, 427–434 (2006). [PubMed: 16879102]
30. Mashima R, Saeki K, Aki D, Minoda Y, Takaki H, Sanada T, Kobayashi T, Aburatani H, Yamanashi Y, Yoshimura A, FLN29, a novel interferon- and LPS-inducible gene acting as a negative regulator of toll-like receptor signaling. J. Biol. Chem. 280, 41289–41297 (2005). [PubMed: 16221674]

31. Villalba M, Bushway P, Altman A, Protein kinase C-theta mediates a selective T cell survival signal via phosphorylation of BAD. J. Immunol. Baltim. Md 1950 166, 5955–5963 (2001).
32. Gruber T, Hermann-Kleiter N, Hinterleitner R, Fresser F, Schneider R, Gastl G, Penninger JM, Baier G, PKC-theta modulates the strength of T cell responses by targeting Cbl-b for ubiquitination and degradation. Sci. Signal. 2, ra30 (2009). [PubMed: 19549985]
33. Dimitrakopoulos GN, Klapa MI, Moschonas NK, PICKLE 3.0: Enriching the human Meta-database with the mouse protein interactome extended via mouse-human orthology. Bioinforma. Oxf. Engl, btaa1070 (2020).
34. Brown EA, Neier SC, Neuhauser C, Schrum AG, Smith SEP, Quantification of Protein Interaction Network Dynamics using Multiplexed Co-Immunoprecipitation. JoVE J. Vis. Exp, e60029 (2019).
35. Schmidt R, Steinhart Z, Layeghi M, Freimer JW, Bueno R, Nguyen VQ, Blaeschke F, Ye CJ, Marson A, CRISPR activation and interference screens decode stimulation responses in primary human T cells. Science 375, eabj4008 (2022). [PubMed: 35113687]
36. Jaeger-Ruckstuhl CA, Hinterbrandner M, Höpner S, Correnti CE, Lüthi U, Friedli O, Freigang S, Sayed M. F. Al, Bührer ED, Amrein MA, Schürch CM, Radpour R, Riether C, Ochsenbein AF, TNIK signaling imprints CD8+ T cell memory formation early after priming. Nat. Commun. 11, 1632 (2020). [PubMed: 32242021]
37. Ikeda F, Deribe YL, Skånland SS, Stieglitz B, Grabbe C, Franz-Wachtel M, van Wijk SJL, Goswami P, Nagy V, Terzic J, Tokunaga F, Androulidaki A, Nakagawa T, Pasparakis M, Iwai K, Sundberg JP, Schaefer L, Rittinger K, Macek B, Dikic I, SHARPIN forms a linear ubiquitin ligase complex regulating NF-κB activity and apoptosis. Nature 471, 637–641 (2011). [PubMed: 21455181]
38. Tokunaga F, Nakagawa T, Nakahara M, Saeki Y, Taniguchi M, Sakata S, Tanaka K, Nakano H, Iwai K, SHARPIN is a component of the NF-κB-activating linear ubiquitin chain assembly complex. Nature 471, 633–636 (2011). [PubMed: 21455180]
39. Oikawa D, Hatanaka N, Suzuki T, Tokunaga F, Cellular and Mathematical Analyses of LUBAC Involvement in T Cell Receptor-Mediated NF-κB Activation Pathway. Front. Immunol. 11, 601926 (2020). [PubMed: 33329596]
40. Abdul-Sater AA, Edilova MI, Clouthier DL, Mbanwi A, Kremmer E, Watts TH, The signaling adaptor TRAF1 negatively regulates Toll-like receptor signaling and this underlies its role in rheumatic disease. Nat. Immunol. 18, 26–35 (2017). [PubMed: 27893701]
41. Lautz JD, Brown EA, Williams VanSchoiack AA, Smith SEP, Synaptic activity induces input-specific rearrangements in a targeted synaptic protein interaction network. J. Neurochem. 146, 540–559 (2018). [PubMed: 29804286]
42. Lautz JD, Gniffke EP, Brown EA, Immendorf KB, Mendel RD, Smith SEP, Activity-dependent changes in synaptic protein complex composition are consistent in different detergents despite differential solubility. Sci. Rep. 9, 10890 (2019). [PubMed: 31350430]
43. Langfelder P, Horvath S, WGCNA: an R package for weighted correlation network analysis. BMC Bioinformatics 9, 559 (2008). [PubMed: 19114008]
44. Heavner WE, Lautz JD, Speed HE, Gniffke EP, Immendorf KB, Welsh JP, Baertsch NA, Smith SEP, Remodeling of the Homer-Shank interactome mediates homeostatic plasticity. Sci. Signal. 14, eabd7325 (2021). [PubMed: 33947797]
45. Lautz JD, Tsegay KB, Zhu Z, Gniffke EP, Welsh JP, Smith SEP, Synaptic protein interaction networks encode experience by assuming stimulus-specific and brain-region-specific states. Cell Rep. 37, 110076 (2021). [PubMed: 34852231]
46. van Oers NS, von Boehmer H, Weiss A, The pre-T cell receptor (TCR) complex is functionally coupled to the TCR-zeta subunit. J. Exp. Med. 182, 1585–1590 (1995). [PubMed: 7595229]
47. Ramello MC, Benzaïd I, Kuenzi BM, Lienlaf-Moreno M, Kandell WM, Santiago DN, Pabón-Saldaña M, Darville L, Fang B, Rix U, Yoder S, Berglund A, Koomen JM, Haura EB, Abate-Daga D, An immunoproteomic approach to characterize the CAR interactome and signalosome. Sci. Signal. 12, eaap9777 (2019). [PubMed: 30755478]
48. Li W, Qiu S, Chen J, Jiang S, Chen W, Jiang J, Wang F, Si W, Shu Y, Wei P, Fan G, Tian R, Wu H, Xu C, Wang H, Chimeric Antigen Receptor Designed to Prevent Ubiquitination and

Downregulation Showed Durable Antitumor Efficacy. Immunity 53, 456–470.e6 (2020). [PubMed: 32758419]

49. Singh N, Frey NV, Engels B, Barrett DM, Shestova O, Ravikumar P, Cummins KD, Lee YG, Pajarillo R, Chun I, Shyu A, Highfill SL, Price A, Zhao L, Peng L, Granda B, Ramones M, Lu XM, Christian DA, Perazzelli J, Lacey SF, Roy NH, Burkhardt JK, Colomb F, Damra M, Abdel-Mohsen M, Liu T, Liu D, Standley DM, Young RM, Brogdon JL, Grupp SA, June CH, Maude SL, Gill S, Ruella M, Antigen-independent activation enhances the efficacy of 4–1BB-costimulated CD22 CAR T cells. Nat. Med. 27, 842–850 (2021). [PubMed: 33888899]
50. Levine BL, Miskin J, Wonnacott K, Keir C, Global Manufacturing of CAR T Cell Therapy. Mol. Ther. Methods Clin. Dev. 4, 92–101 (2016). [PubMed: 28344995]
51. Ravanpay AC, Gust J, Johnson AJ, Rolczynski LS, Cecchini M, Chang CA, Hoglund VJ, Mukherjee R, Vitanza NA, Orentas RJ, Jensen MC, EGFR806-CAR T cells selectively target a tumor-restricted EGFR epitope in glioblastoma. Oncotarget 10, 7080–7095 (2019). [PubMed: 31903167]
52. Wei Q, Brzostek J, Sankaran S, Casas J, Hew LS-Q, Yap J, Zhao X, Wojciech L, Gascoigne NRJ, Lck bound to coreceptor is less active than free Lck. Proc. Natl. Acad. Sci. 117, 15809–15817 (2020). [PubMed: 32571924]
53. Li L, Guo X, Shi X, Li C, Wu W, Yan C, Wang H, Li H, Xu C, Ionic CD3−Lck interaction regulates the initiation of T-cell receptor signaling. Proc. Natl. Acad. Sci. 114, E5891–E5899 (2017). [PubMed: 28659468]
54. Lo W-L, Shah NH, Ahsan N, Horkova V, Stepanek O, Salomon AR, Kuriyan J, Weiss A, Lck promotes Zap70-dependent LAT phosphorylation by bridging Zap70 to LAT. Nat. Immunol. 19, 733–741 (2018). [PubMed: 29915297]
55. Park HH, Structure of TRAF Family: Current Understanding of Receptor Recognition. Front. Immunol. 9 (2018).
56. Vanamee ÉS, Faustman DL, Structural principles of tumor necrosis factor superfamily signaling. Sci. Signal. 11, eaao4910 (2018). [PubMed: 29295955]
57. Zheng C, Kabaleeswaran V, Wang Y, Cheng G, Wu H, Crystal structures of the TRAF2: cIAP2 and the TRAF1: TRAF2: cIAP2 complexes – affinity, specificity and regulation. Mol. Cell 38, 101–113 (2010). [PubMed: 20385093]
58. Ceccarelli A, Di Venere A, Nicolai E, De Luca A, Minicozzi V, Rosato N, Caccuri AM, Mei G, TNFR-Associated Factor-2 (TRAF2): Not Only a Trimer. Biochemistry 54, 6153–6161 (2015). [PubMed: 26390021]
59. Ye H, Park YC, Kreishman M, Kieff E, Wu H, The Structural Basis for the Recognition of Diverse Receptor Sequences by TRAF2. Mol. Cell 4, 321–330 (1999). [PubMed: 10518213]
60. Ye H, Wu H, Thermodynamic characterization of the interaction between TRAF2 and tumor necrosis factor receptor peptides by isothermal titration calorimetry. Proc. Natl. Acad. Sci. U. S. A. 97, 8961–8966 (2000). [PubMed: 10908665]
61. Davenport AJ, Cross RS, Watson KA, Liao Y, Shi W, Prince HM, Beavis PA, Trapani JA, Kershaw MH, Ritchie DS, Darcy PK, Neeson PJ, Jenkins MR, Chimeric antigen receptor T cells form nonclassical and potent immune synapses driving rapid cytotoxicity. Proc. Natl. Acad. Sci. 115, E2068–E2076 (2018). [PubMed: 29440406]
62. Dong R, Libby KA, Blaeschke F, Fuchs W, Marson A, Vale RD, Su X, Rewired signaling network in T cells expressing the chimeric antigen receptor (CAR). EMBO J. 39, e104730 (2020). [PubMed: 32643825]
63. Kang SW, Wahl MI, Chu J, Kitaura J, Kawakami Y, Kato RM, Tabuchi R, Tarakhovsky A, Kawakami T, Turck CW, Witte ON, Rawlings DJ, PKCbeta modulates antigen receptor signaling via regulation of Btk membrane localization. EMBO J. 20, 5692–5702 (2001). [PubMed: 11598012]
64. Sun C, Shou P, Du H, Hirabayashi K, Chen Y, Herring LE, Ahn S, Xu Y, Suzuki K, Li G, Tsahouridis O, Su L, Savoldo B, Dotti G, THEMIS-SHP1 Recruitment by 4–1BB Tunes LCK-Mediated Priming of Chimeric Antigen Receptor-Redirected T Cells. Cancer Cell 37, 216–225.e6 (2020). [PubMed: 32004441]

65. Edilova MI, Abdul-Sater AA, Watts TH, TRAF1 Signaling in Human Health and Disease. Front. Immunol. 9, 2969 (2018). [PubMed: 30619326]

66. McPherson AJ, Snell LM, Mak TW, Watts TH, Opposing roles for TRAF1 in the alternative versus classical NF-κB pathway in T cells. J. Biol. Chem. 287, 23010–23019 (2012). [PubMed: 22570473]

67. Davis TR, Schrum AG, IP-FCM: Immunoprecipitation Detected by Flow Cytometry. JoVE J. Vis. Exp, e2066 (2010).

68. Leek JT, Johnson WE, Parker HS, Jaffe AE, Storey JD, The sva package for removing batch effects and other unwanted variation in high-throughput experiments. Bioinforma. Oxf. Engl. 28, 882–883 (2012).

69. Voineagu I, Wang X, Johnston P, Lowe JK, Tian Y, Horvath S, Mill J, Cantor RM, Blencowe BJ, Geschwind DH, Transcriptomic analysis of autistic brain reveals convergent molecular pathology. Nature 474, 380–384 (2011). [PubMed: 21614001]

70. Bayne RS, Puckett S, Rodrigues LU, Cramer SD, Lee J, Furdui CM, Chou JW, Miller LD, Ornelles DA, Lyles DS, MAP3K7 and CHD1 Are Novel Mediators of Resistance to Oncolytic Vesicular Stomatitis Virus in Prostate Cancer Cells. Mol. Ther. - Oncolytics 17, 496–507 (2020). [PubMed: 32529027]

71. Buchl SC, Hanquier Z, Haak AJ, Thomason YM, Huebert RC, Shah VH, Maiers JL, Traf2 and NCK Interacting Kinase Is a Critical Regulator of Procollagen I Trafficking and Hepatic Fibrogenesis in Mice. Hepatol. Commun. 6, 593–609 (2022). [PubMed: 34677004]

72. Lee S-H, Mayr C, Gain of Additional BIRC3 Protein Functions through 3′-UTR-Mediated Protein Complex Formation. Mol. Cell 74, 701–712.e9 (2019). [PubMed: 30948266]

73. Kreckel J, Anany MA, Siegmund D, Wajant H, TRAF2 Controls Death Receptor-Induced Caspase-8 Processing and Facilitates Proinflammatory Signaling. Front. Immunol. 10 (2019).

74. Thys A, Trillet K, Rosińska S, Gayraud A, Douanne T, Danger Y, Renaud CCN, Antigny L, Lavigne R, Pineau C, Com E, Vérité F, Gavard J, Bidère N, Serine 165 phosphorylation of SHARPIN regulates the activation of NF-κB. iScience 24, 101939 (2021). [PubMed: 33392484]

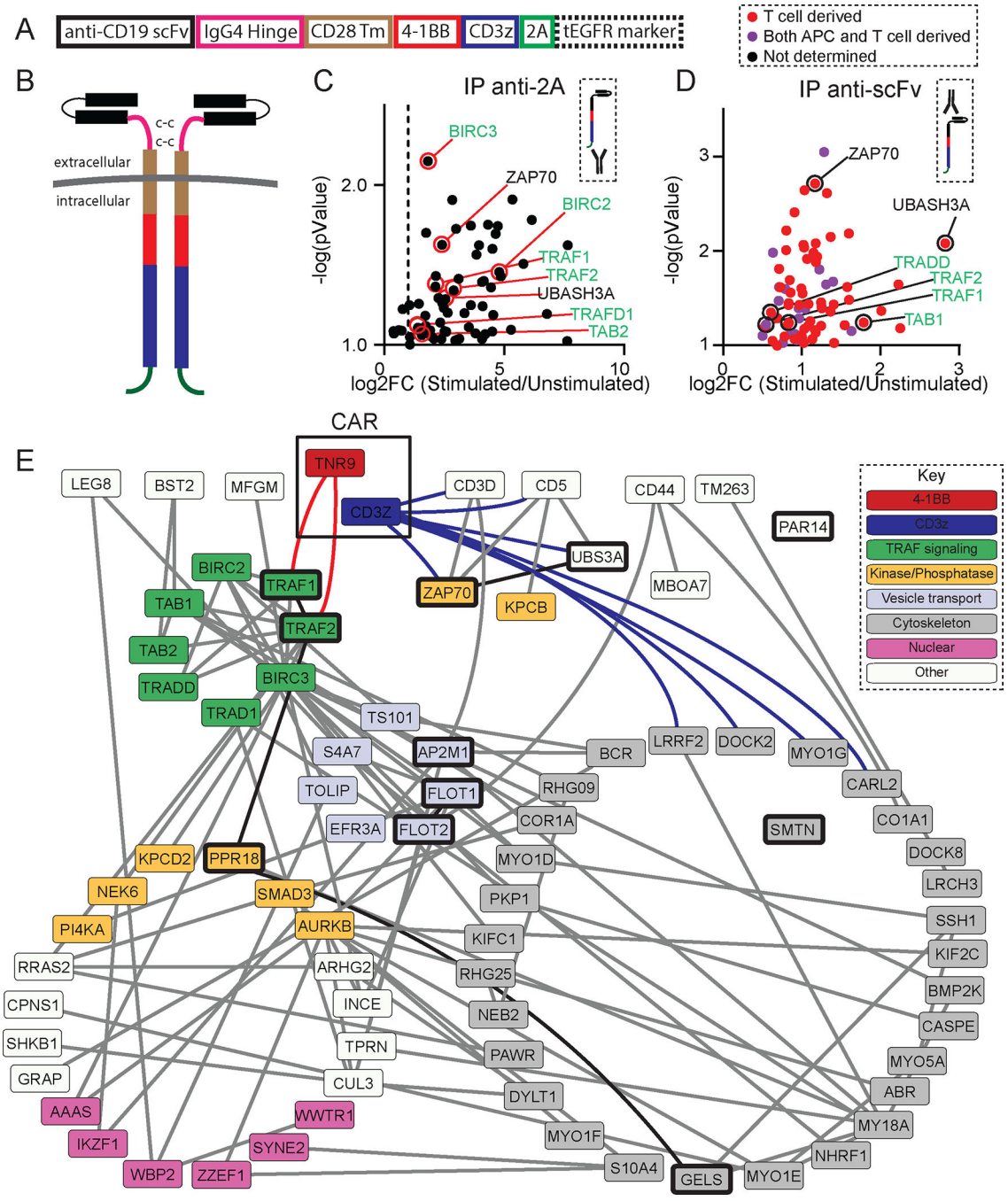

Fig. 1. Activity-dependent bbζCAR CAR interactome identified by IP-MS.

(**A**) Schematic representation of the bbζCAR construct. (**B**) Domain model of the mature CAR. Domain colors correspond to those used in (A). (**C**) Volcano plot showing all of the proteins that were significantly enriched in stimulated vs. unstimulated CARs immunoprecipitated with an antibody against the C-terminal 2A tag, with selected proteins labeled. Green type indicates TRAF signaling proteins. Data are from 22 samples derived from four individuals: three CD8CAR, four CD4CAR, and four mock-transduced T cell cultures, each stimulated and unstimulated. (**D**) Volcano plot showing all of the proteins

that were significantly enriched in stimulated vs. unstimulated CARs immunoprecipitated with an antibody against the N-terminal scFv domain, with selected proteins labeled. Green type indicates TRAF signaling proteins. Dot color indicates the cellular origin of the protein as determined by isotopic labeling; APC-derived proteins are not shown. Data are from 16 total samples from four individuals: 4 CD4CAR stimulated samples, 4 CD4CAR unstimulated samples, and IgG immunoprecipitation controls for each. (E) Known protein-protein interactions among the proteins identified in (C) and (D). Node color indicates the protein family, as indicated in the key, and thick outlines indicate proteins identified in both independent experiments. Red edges indicate known interactions with 4–1BB, blue edges indicate known interactions with CD3ζ, and bold edges indicate interactions among proteins identified in both experiments. Note that proteins that were identified in only one of the two experiments and have no database-documented interactions are not shown.

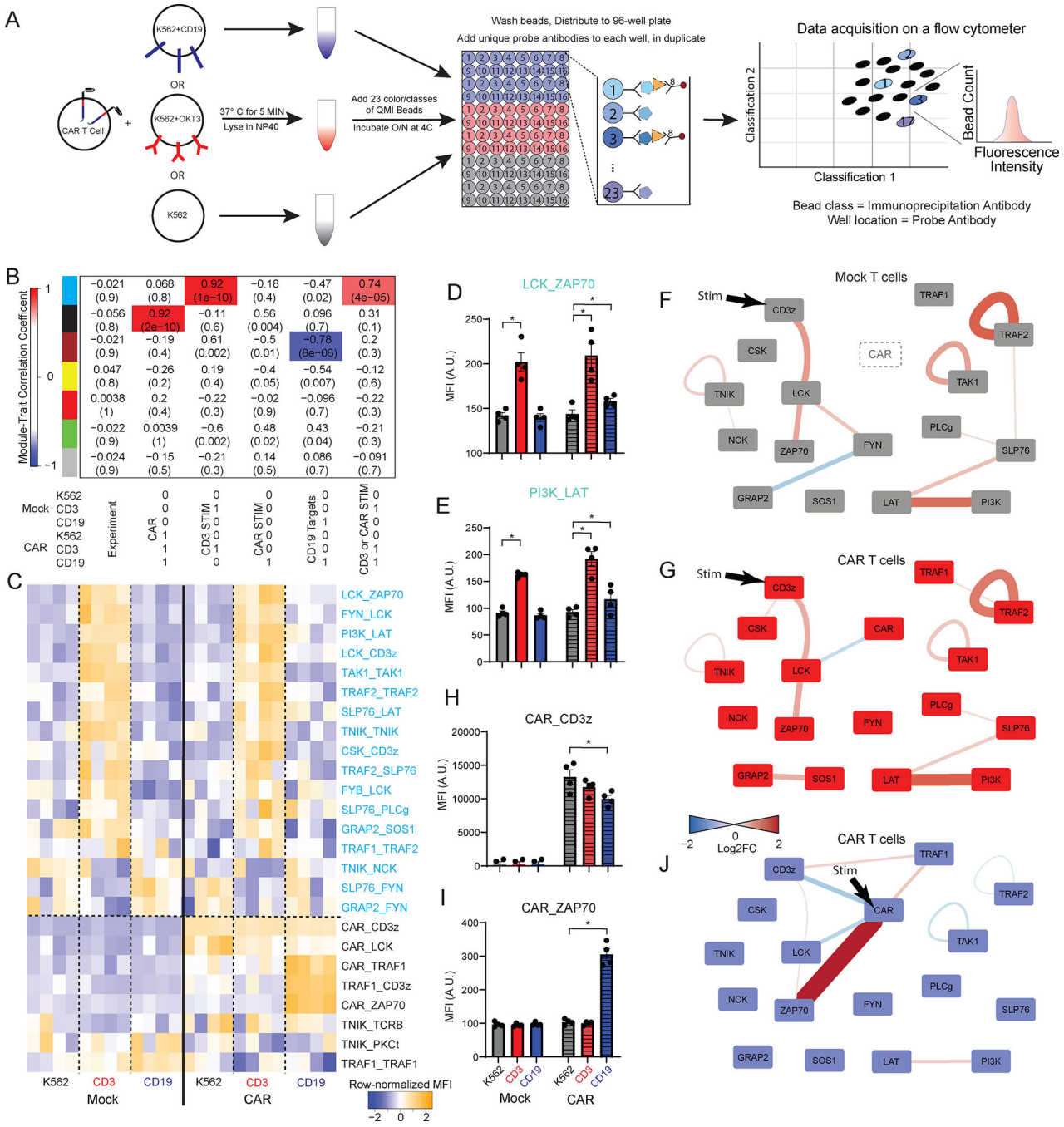

Fig. 2. Activity-dependent bbζCAR protein-protein interactions identified by QMI.

(**A**) Experimental design showing CAR T cell stimulation, NP-40 lysis, and quantitative multiplex co-immunoprecipitation (QMI). (**B**) Module-trait correlation table reports the correlation coefficients and p-values (in parentheses) between the eigenvector of each color-coded CNA module (colored boxes) and a binary description of experimental variables, which are listed below the table. Module-trait correlations > 0.7 are highlighted in red (positive correlations) whereas those < −0.7 are highlighted in blue (negative correlations). (**C**) Row-normalized heatmap of the median fluorescence intensity (MFI) of protein-protein

interactions that significantly changed after CD3 or CD19 stimulation. Interaction color indicates membership in the “TCR stimulation” (turquoise) or “CAR” (bIack) CNA modules. (**D** and **E**) MFI values of (D) LCK_ZAP70 and (E) PI3K_LAT, representative of the “TCR stimulation” module, which increased after anti-CD3 stimulation and increased to a lesser degree after CD19 stimulation. *$P < 0.05$ by ANC. (**F** and **G**) Node-edge diagrams of interactions that changed with anti-CD3 stimulation in (F) mock-transduced or (G) CAR T cells. Edges represent a change in the MFI of an interaction between the connected nodes; edge color and width indicate the direction and magnitude of the change, respectively. (**H** and **I**) MFI values of (H) CAR_CD3 and (I) CAR_ZAP70, which are both in the “CAR” module. *$P < 0.05$ by ANC. (**J**) Interactions that changed with CD19 stimulation in CAR T cells. All data are from four experiments performed on cells manufactured from a single donor.

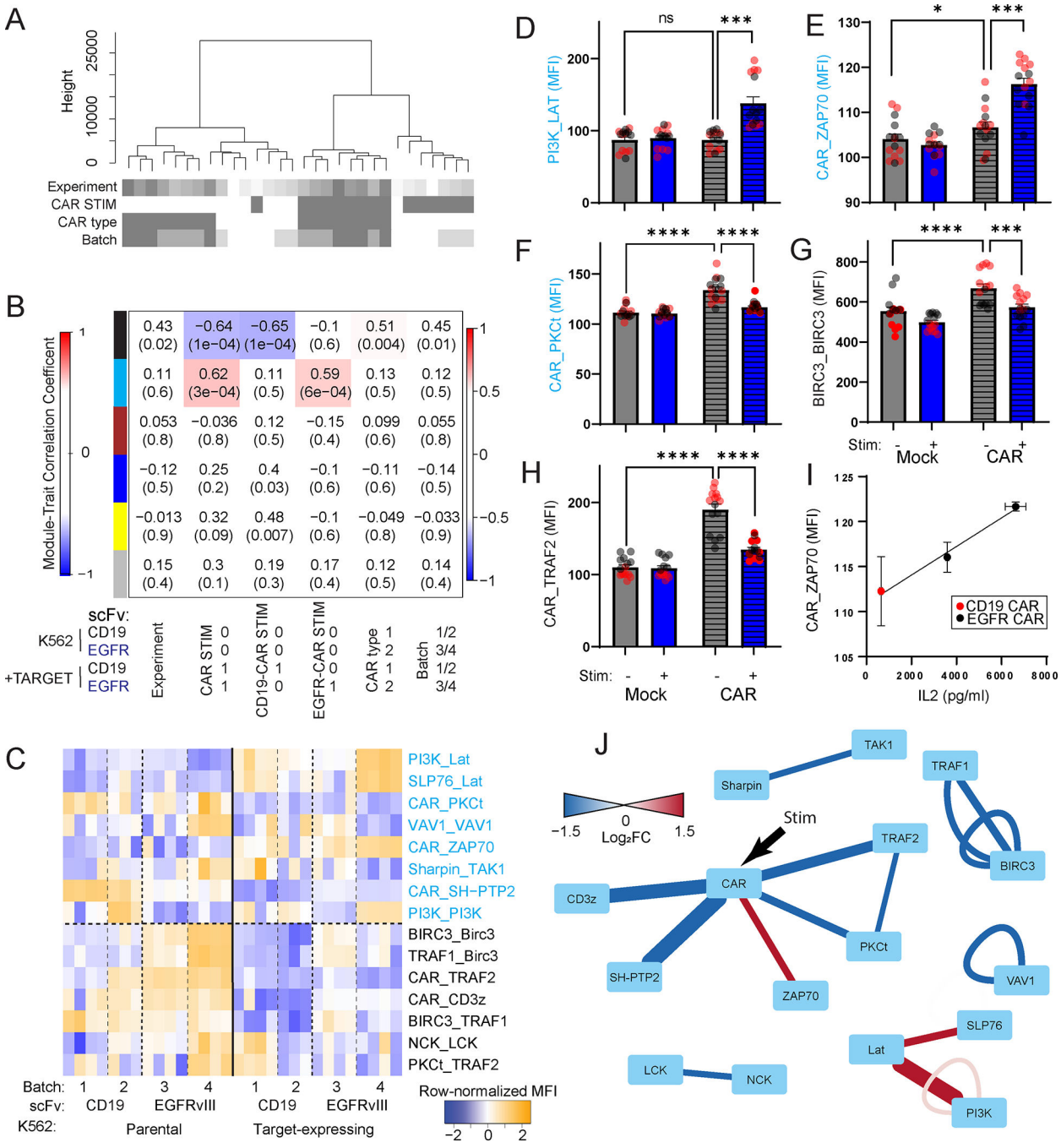

Fig. 3. Consistent bbζCAR signaling despite batch- and target-specific variabilities.

(**A** to **J**) Four batches of BBζ CAR T cells, with two different scFv targets, were manufactured from a single donor and lysed in digitonin. (A) Hierarchical clustering of all detected interactions shows clustering by stimulation, then by CAR type, then batch. (B) A module-trait correlation table reports the correlation coefficients and p-values (in parentheses) between the eigenvector of each coIor-coded CNA module (colored boxes) and a binary description of the experimental variables, which is below the table. Module-trait correlations > 0.5 are highlighted with red (positive correlations), whereas those

correlations < −0.5 are highlighted with blue (negative correlations). (C) Row-normalized heatmap of ANCՈCNA-significant interactions in the turquoise or black modules. (D to H) MFI values of (D) PI3K_LAT, (E) CAR_ZAP70, and (F) CAR_PKCΦ, members of the turquoise module, and (G) BIRC3_BIRC3 and (H) CAR_TRAF2, members of the black module, after CD19 stimulation of mock-transduced or bbζCAR T cells. $*P < 0.05$ by one-way ANOVA followed by Sidak's multiple comparison test. (I) Correlation between the MFI of CAR_ZAP70 and the amount of IL-2 in the culture medium after 18 hours of CD19-stimulation of CAR T cells. (J) Node-edge diagram showing interactions that were significantly changed (as determined by ANCՈCNA) after bbζCAR target engagement. Edges represent a change in the extent of the interaction between the connected nodes; edge color and width indicate the direction and magnitude of the change, respectively. Data are from 60 biological replicates, with 15 per condition. Only CAR+ cells (N = 15 unstimulated and N = 15 stimulated) are represented in (A) to (C) and (J).

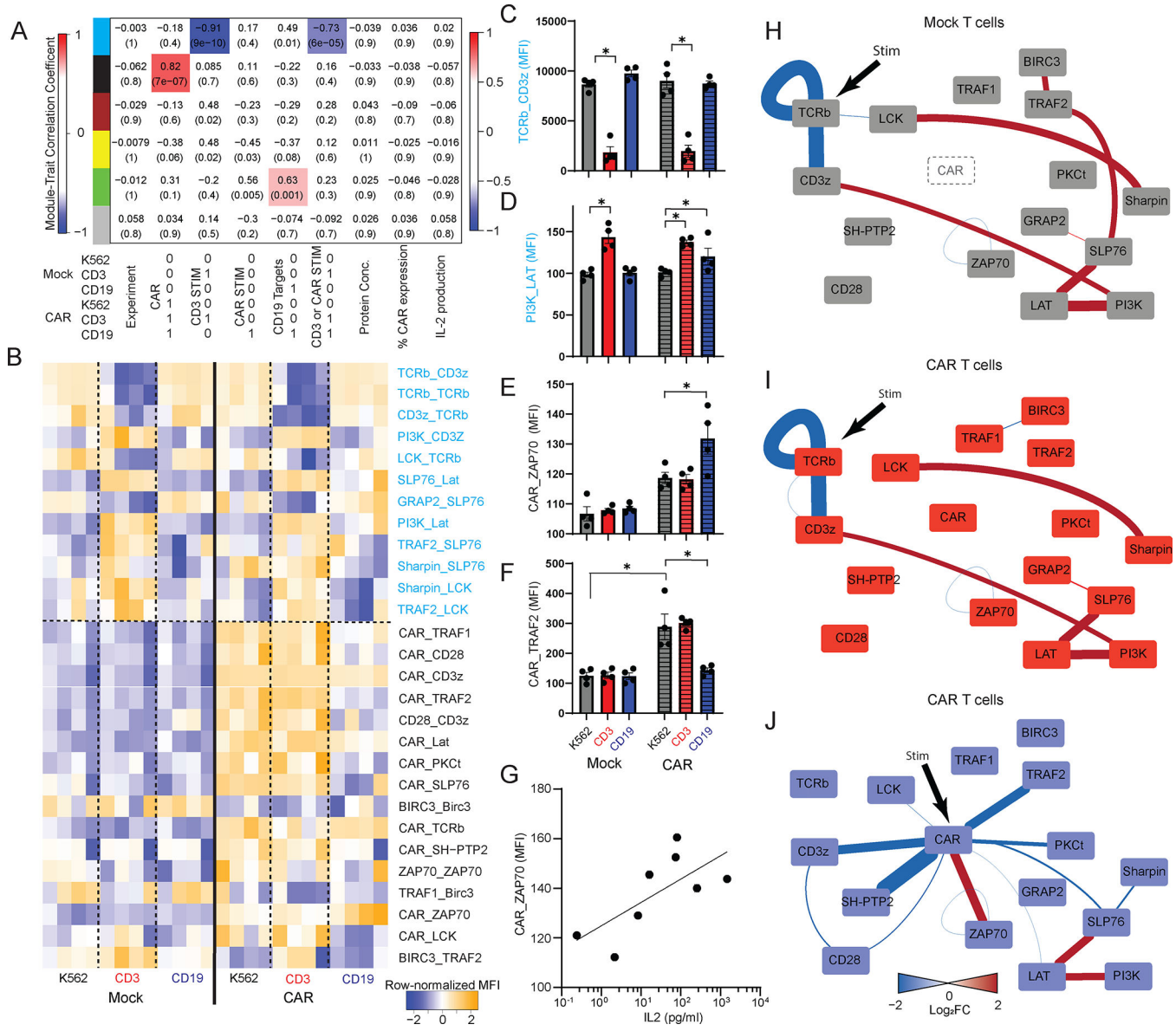

Fig. 4. CAR signalosome dynamics are consistent among donors and correlate with IL-2 secretion.

(**A** to **J**) Four batches of anti-CD19 bbζCARs were produced from four separate donors and were lysed in digitonin. (A) A module-trait correlation table reports the correlation coefficients and p-values (in parenthesis) between the eigenvector of each color-coded CNA module (colored boxes) and a binary description of experimental variables, which is below the table. Module-trait correlations >0.6 are highlighted with red (positive correlations), whereas those < 0.6 are highlighted with blue (negative correlations). (B) Row-normalized heatmap of ANCՈCNA-significant interactions in the “TCR-stim” (turquoise) or “CAR” (black) modules. Data are grouped by mock or CAR T cells (indicated by the solid black line), then by target type (indicated by the dashed lines); the first column after each line represents matched conditions from donor 1, the second donor 2, etc. (C to F) MFI values of (C) TCR_CD3ζ and (D) PI3K_LAT, members of the turquoise module, and (E)

CAR_ZAP70 and (F) CAR_TRAF2, members of the black module, after CD19 stimulation of mock-transduced or bbζCAR T cells. *$P < 0.05$ by ANC. (G) Correlation between the MFI of CAR_ZAP70 and the amount of IL-2 in the culture medium after 18 hours of CD19-stimulation of in CAR T cells. Data are from eight individual donors. (H to J) Node-edge diagram showing interactions that were significantly changed (as determined by ANC∩CNA) after anti-CD3 stimulation in (G) mock-transduced or (H) CAR T cells, or (I) CD19 stimulation in CAR T cells. Edges represent a change in the amount of interaction between the connected nodes; edge color and width indicate the direction and magnitude of the change, respectively. Data are from 24 biological replicates, with four per condition, derived from four different, de-identified healthy donors.

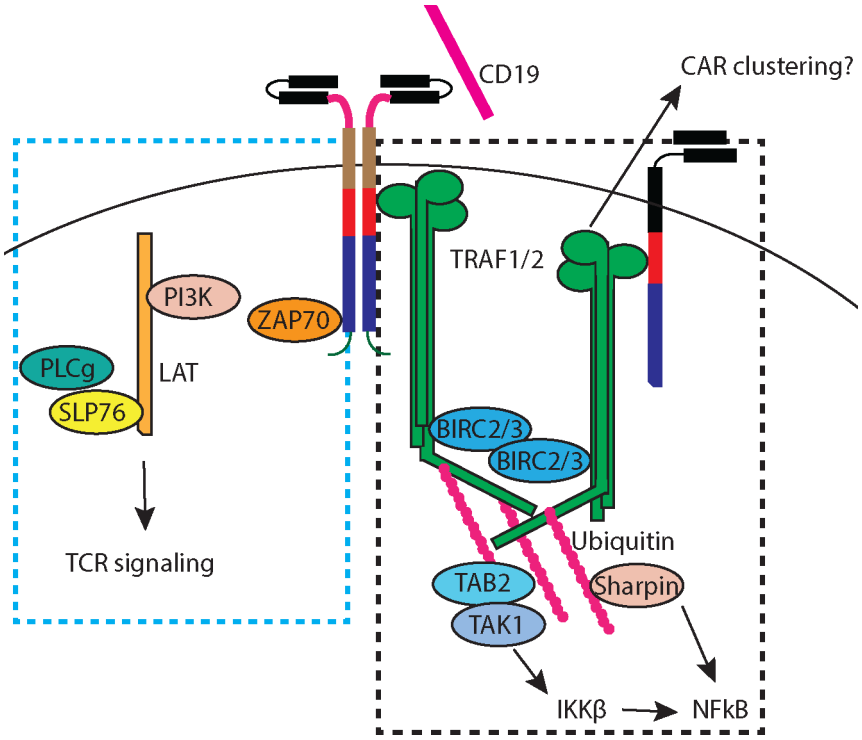

Fig. 5. Modular organization of CAR signaling.

Upon CD19 engagement, the bbζCAR engages two modules (surrounded by dashed boxes), one composed of SLP76-LAT-PI3K signaling complexes that mimics TCR signaling, the other composed of TRAF signaling complexes that initiates NF-κB signaling.